

Dual-Source Energy Harvesting System using TDM with Dynamic MPPT and Wide-Range ZCS

Yehia Hamdy Yehia, Hesham Omran, and Sameh A.Ibrahim
 Electronics and Communication Engineering Department, Ain Shams university
 Cairo, Egypt
 E-mail: yahya.hamdy.yahya@gmail.coml

Abstract—This paper presents an efficient dynamic technique for energy combining from thermoelectric generators (TEG) and piezoelectric transducers (PZ). A dual-source maximum-power-point-tracking (MPPT) unit working in analogues way to phase-locked loops (PLL) is proposed. The dynamic MPPT achieves global maximum power extraction by matching both sources impedance varying from 1.5Ω to 43Ω for a thermoelectric generator cell and from $2 \text{ k}\Omega$ to $44 \text{ k}\Omega$ for a piezoelectric cell with only 2% power loss. A wide-range zero-current-switching (WR-ZCS) circuit is proposed to tune inductor discharging time with a good resolution using a digitally-tuned delay cell providing 30 ns and 100 ns delays. With an output control unit and with the aid of a kick start voltage a self-biased operation is obtained while the output voltage is regulated at 2.5 V.

Index Terms—Thermoelectric Generator (TEG), Piezoelectric (PZ) Transducers, Time Division Multiplexing (TDM), Dual Maximum Power Point Tracking (MPPT), Energy Harvesting (EH), Wide Range Zero Current Switching (WR-ZCS)

I. INTRODUCTION

Modern wireless sensors carry-on sophisticated operations like; sensing, processing and wireless transmission, while using a limited energy budget. Energy harvesting (EH) techniques gained a recent interest to increase the reliability and life time of these nodes. For example, [1] and [2] have focused on implementing low-power EH units to provide an interface between single energy sources and wireless nodes. As monitoring systems in industrial locations become more complex and autonomous, wireless nodes are going to be more power consuming. In order to increase such systems robustness and sustainability, energy combining from different energy sources using time division multiplexing (TDM) provides an adequate solution. In [3], an inductor sharing technique is used to combine energy from different sources using a hard-coded pattern generator providing a small form-factor implementation. In [4], an energy harvesting system is introduced to combine available energy from a piezoelectric (PZ) transducer and a photovoltaic (PV) cell.

One main concern is to maintain these energy sources at their maximum power points (MPP) to achieve maximum efficiency at wide-range of sources impedance. Many techniques were proposed to track impedance variations. In [5], dynamic maximum-power-point-tracking (MPPT) unit is implemented to track immediate impedance variations in a thermoelectric generator (TEG) array. Moreover in [6], external control signals are used to adjust MPP operation for optimum solar

harvesting. Despite many publications on impedance tracking, dynamic impedance matching for dual-source harvesting systems employing TDM is not developed yet.

This work presents an efficient technique for energy combining using a dynamic impedance matching unit. An efficient step-up converter working in discontinuous conduction mode (DCM) extracts energy from a (TEG) cell and a (PZ) transducer using a single off-chip inductor. The Proposed MPPT unit controls the converter-input impedance (Z_{in}) dynamically to match the impedance variations from 1.5Ω to 43Ω for a TEG cell also from $2 \text{ k}\Omega$ to $44 \text{ k}\Omega$ for a PZ cell with only 2% power loss. A wide-range zero current switching (WR-ZCS) circuit is proposed to control inductor current in DCM for both sources. The mathematical analysis for the proposed architecture is performed to derive analytical expressions for the input-impedance seen by each energy source to control their operating voltages.

The rest of the paper is organized as follows: Section II shows the proposed system architecture. Section III shows the control scheme implementation of the MPPT, WR-ZCS and the output regulation unit. Section IV presents the simulation results. Section V concludes the paper.

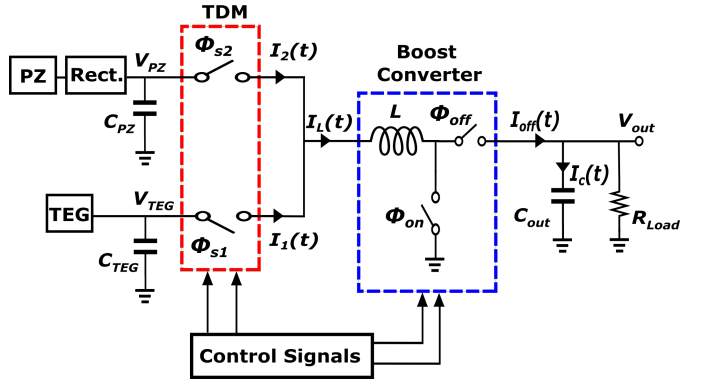


Fig. 1: Combining energy from different energy sources using TDM

II. PROPOSED SYSTEM ARCHITECTURE

A TEG cell and a PZ transducer with an off-chip rectifier are used as inputs to the boost converter shown in Fig. 1. While C_{TEG} and C_{PZ} are used to smoothen energy sources operating voltages, C_{out} is used to provide low-ripple dc output volt-

age V_{out} . TDM is applied by periodically switching between the TEG cell and the PZ cell in order to combine the harvested energy at the output load. V_{TEG} and V_{PZ} represent sources voltages stored on C_{TEG} and C_{PZ} , respectively. While ϕ_{s1} and ϕ_{s2} represent control signals for source selection, ϕ_{on} and ϕ_{off} represent control signals for inductor charging and discharging, respectively. In Fig. 2, source selection signals ϕ_{s1} and ϕ_{s2} and inductor current control signals ϕ_{on} and ϕ_{off} are all shown in a complete harvesting cycle T_{CLK} . m and n represent the number of inductor charging and discharging cycles for each harvester during its allocated time αT_{CLK} and $(1 - \alpha)T_{CLK}$, respectively, where α represents TDM factor. $I_1(t)$ and $I_2(t)$ represent current waveforms for TEG and PZ sources. While $I_L(t)$ represents the inductor (L) current, $I_{off}(t)$ represents the load current. T_{on1} and T_{on2} represent the time spent in charging the inductor for each energy source, T_{off1} and T_{off2} represent the corresponding required times for inductor complete discharging. During on-times, inductor current ramps up linearly to max values I_{p1} during TEG harvesting and I_{p2} during PZ harvesting, while during off-times it ramps down increasing the output voltage. Let D_1 and D_2 represent duty cycles of the charging signals for the TEG cell and the PZ cell, respectively. The equivalent impedance seen by each source can be viewed as the ratio between its operating voltage and the average current drawn from the source in a complete harvesting cycle [3].

The average drawn current from the TEG cell can be written as follows

$$\bar{I}_1 = \frac{\int_0^{T_{CLK}} I_1(t) dt}{T_{CLK}} = \frac{\alpha^2 D_1^2 V_{TEG} \left(1 + \frac{T_{off1}}{T_{on1}}\right)}{2mL f_{CLK}}. \quad (1)$$

The average drawn current from the PZ cell can be written in the same manner as follows

$$\bar{I}_2 = \frac{\int_0^{T_{CLK}} I_2(t) dt}{T_{CLK}} = \frac{(1 - \alpha)^2 D_2^2 V_{PZ} \left(1 + \frac{T_{off2}}{T_{on2}}\right)}{2nL f_{CLK}}. \quad (2)$$

From (1) and (2), equivalent resistance seen by each source can be written as

$$R_{IN.TEG} = \frac{V_{TEG}}{\bar{I}_1} = \frac{2mL f_{CLK}}{\alpha^2 D_1^2 \left(1 + \frac{T_{off1}}{T_{on1}}\right)} \quad (3)$$

and

$$R_{IN.PZ} = \frac{V_{PZ}}{\bar{I}_2} = \frac{2nL f_{CLK}}{(1 - \alpha)^2 D_2^2 \left(1 + \frac{T_{off2}}{T_{on2}}\right)}. \quad (4)$$

As the converter is working in DCM, T_{off1} and T_{off2} can be neglected with respect to T_{on1} and T_{on2} at higher conversion ratios [5].

In order to make the matching algorithm linear, fixed duty-cycle D_1 and D_2 is used for the control signals. Commercial TEG cells have a very-low resistance range than PZ transducers with off-chip rectifiers [3]. With D_1 of 50% and D_2 of 6.25% the boost converter matches TEG and PZ different input impedance ranges with a less sophisticated implementation. At normal conditions, TEG cells have higher-energy density

than PZ cells. However, in high-vibration working areas, PZ sources can guarantee system continuous operation. A power calculation unit can be used for adaptive TDM, but this imposes an extra overhead on power consumption. As a result, fixed TDM is employed using TDM factor α of 0.5. Converter switches are properly sized to avoid inductor current saturation with minimized static and switching losses. Using L of 50 μ H and f_{CLK} of 1.25 kHz, the entire range for both sources impedance is covered with an optimum converter efficiency.

With these numbers and assumptions, (3) and (4) can be rewritten as

$$R_{IN.TEG} = 2m \quad (5)$$

and

$$R_{IN.PZ} = 128n. \quad (6)$$

Form (5) and (6), the proposed MPPT matching range for both TEG and PZ sources is illustrated in Table I. In table I, while f_{TEG} and f_{PZ} are the generated frequencies to control switching frequency for the TEG and the PZ harvesting, f_{CLK} is the main system clock. M_{TEG} and N_{PZ} are the programmable-division ratios. In order to obtain MPP operation for both sources, MPPT dynamically changes the effective harvesting frequency for each source. This is done by changing the division ratios M_{TEG} and N_{PZ} of both f_{TEG} and f_{PZ} , respectively. More details will be explained in section III

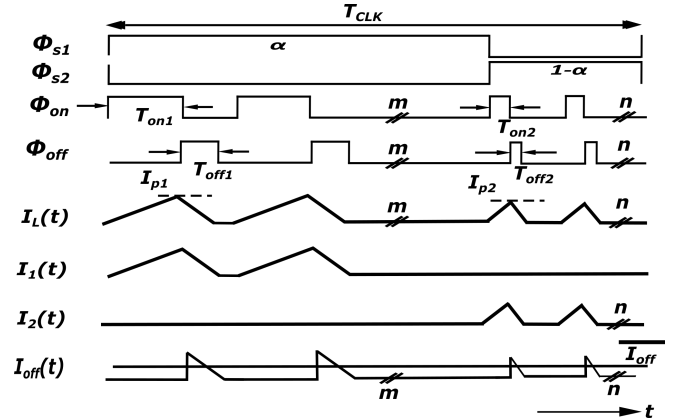


Fig. 2: Timing signals and current waveforms for boost converter in a complete T_{CLK} cycle

III. CONTROL SCHEME IMPLEMENTATION

A. MPPT Mechanism

Impedance matching for both energy sources guarantees maximum power to be delivered to the load [7]–[10]. For a TEG cell, maximum power extraction is achieved by maintaining its closed voltage V_{TEG} at half of its open-circuit voltage $V_{TEG,OC}$. Moreover, for a PZ cell with a rectifier, the MPP is also achieved by regulating the operating voltage V_{PZ} at half of its open-circuit voltage $V_{PZ,OC}$ [3].

A simplified schematic for the proposed system architecture is shown in Fig. 3a. The energy sources are connected to the

TABLE I: MPPT Matching Range

(a) TEG input matched impedance

M_{TEG}	$m = \frac{f_{TEG}}{2 \cdot f_{CLK} \cdot M_{TEG}}$	$R_{IN,TEG}$	2% losses range
32	1	2Ω	$1.5\Omega - 2.66\Omega$
16	2	4Ω	$3\Omega - 5.32\Omega$
8	4	8Ω	$6\Omega - 10.64\Omega$
4	8	16Ω	$12\Omega - 21.28\Omega$
2	16	32Ω	$24\Omega - 42.56\Omega$

(b) PZ input matched impedance

N_{PZ}	$n = \frac{f_{PZ}}{2 \cdot f_{CLK} \cdot N_{PZ}}$	$R_{IN,PZ}$	2% losses range
32	16	2048Ω	$1536\Omega - 2723\Omega$
16	32	4096Ω	$3072\Omega - 5440\Omega$
8	64	8192Ω	$6144\Omega - 10985\Omega$
4	128	16384Ω	$12288\Omega - 21790\Omega$
2	256	32768Ω	$24576\Omega - 44000\Omega$

boost converter through M_{s1} and M_{s2} and controlled by ϕ_{s1} and ϕ_{s2} . For DCM operation WR-ZCS is employed between V_{out} and V_{ind} nodes in order to generate the required ϕ_{off} signal to control M_{p1} . Moreover, while WR-ZCS guarantees DCM operation, MPPT unit guarantees dynamic impedance matching by adjusting ϕ_{on} to control M_{n1} . Meanwhile, the output voltage is stored on C_{out} with R_{load} representing the output load, the wireless circuit is controlled by an enable signal EN and it is heavily duty-cycled based on the output voltage condition.

In Fig. 3b, fixed duty-cycle frequency modulation (FM) technique is implemented using low-power programmable dividers which are controlled by MPPT in order to adjust ϕ_{on} signal for M_{n1} . All timing signals are generated using an oscillator of 5.12 MHz with V_{out} as a supply. Dedicated by-2 dividers are used to generate f_{PZ} , f_{TEG} and f_{CLK} . Moreover, dead-time circuit generates non-overlapping clock phases ϕ_{s1} and ϕ_{s2} for TDM operation. The MPPT unit consists of a dual-fractional-open-circuit-voltage (FOCV) extraction unit alongside with an INC/DEC logic all controlled with a control-logic unit. While the control logic generates all the required signals for the extraction unit, dual-FOCV is responsible for sampling and generating the optimum-operating points $V_{TEG-MPP}$ and V_{PZ-MPP} . INC/DEC logic periodically compares sources operating voltages V_{TEG} and V_{PZ} against their corresponding generated optimum points to precisely control ϕ_{on} by either increasing or decreasing the current division-ratios. This algorithm works in an analogues way to phase locked loops (PLL) but with the generated frequency is being controlled by digital logic circuits.

The proposed dual-FOCV extraction unit is shown in Fig. 4a. This unit obtains MPP operation firstly by charging C_{max1} to $V_{TEG,OC}$ during ϕ_{sa1} through M_2 , also by charging C_{max2} to $V_{PZ,OC}$ during ϕ_{sa2} through M_1 . This is done by ϕ_{in1} and ϕ_{in2} to disengage M_8 and M_7 from the harvesters.

During the sampling phase, a refreshing process is necessary to ensure a complete discharge of C_{sh1} and C_{sh2} to be ready for the upcoming charge sharing phase and this is done by ϕ_{refr1} and ϕ_{refr2} through M_6 and M_5 . After the sampling and

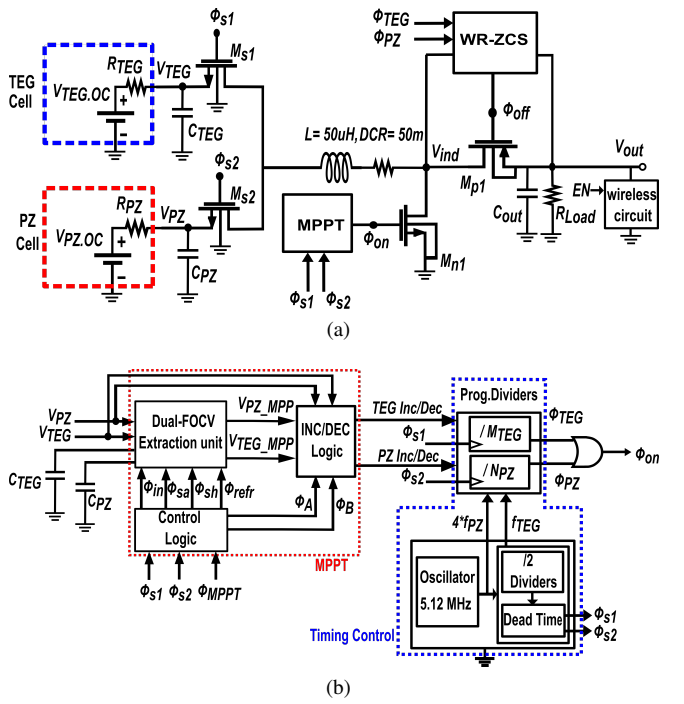
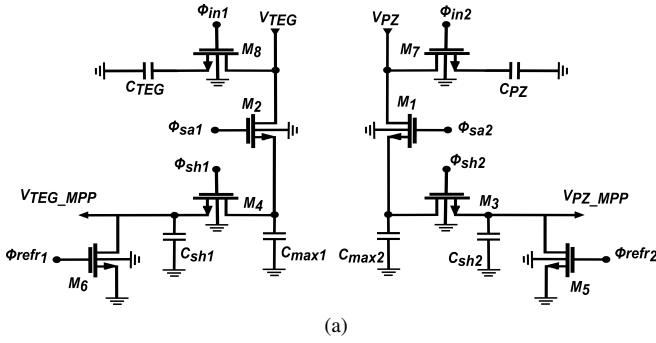


Fig. 3: (a) Boost converter employing TDM Technique with WR-ZCS and MPPT (b) Ton Control Circuits

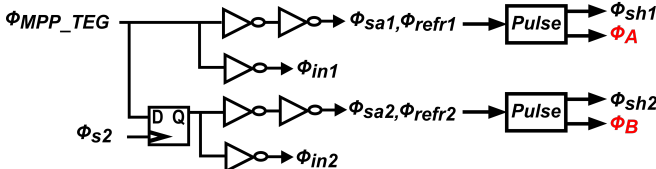
the refreshing phase, a charge sharing phase occurs between C_{max1} and C_{sh1} through M_4 and between C_{max2} and C_{sh2} through M_3 , yielding the current MPP for both harvesters. This procedure is repeated every MPPT cycle to track sources variations. C_{max1} and C_{max2} also C_{sh1} and C_{sh2} can be integrated on-chip and equal to 30 pF each, while $CTEG$ and CPZ are off-chip and chosen based on the max allowed ripples at both sources input. As ripples are maximum at the lowest-input impedance for both sources which is 1.5Ω in case of the TEG cell and $2k\Omega$ in case of the PZ cell, thus choosing $CTEG$ of $470\mu F$ and CPZ of $1\mu F$ guarantees max ripples of only $\pm 13.5\text{ mV}$ and $\pm 26.7\text{ mV}$ for both V_{TEG} and V_{PZ} , respectively. MPPT control logic circuit and waveforms for all switches matrix $M_1 - M_8$ are illustrated in Fig. 4b.

Every MPPT cycle, after the charge sharing phase and during ϕ_A and ϕ_B , both V_{TEG} and V_{PZ} are compared with their corresponding MPP values using Strong-ARM comparators. In order to meet both sources impedance variation, result is latched and fed into an INC/DEC logic unit to either increase or decrease M_{TEG} or N_{PZ} for the next harvesting cycle as shown in Fig. 5a.

50% duty-cycle programmable divider operating from f_{TEG} is implemented and controlled by a 4-bit register to select the required output frequency from $f/2$, $f/4$, $f/8$, $f/16$ and $f/32$. Moreover, in Fig. 5b, a 6.25% duty-cycle divider working directly from the oscillator-output frequency is also implemented. An and array is used to generate the required duty-cycle. Dividers power scale dynamically with the available energy from the harvesters by selecting only higher-frequency dividers at higher harvesters impedance. This is



(a)



(b)

Fig. 4: (a) MPPT switch matrix circuit (b) MPPT control logic circuit and waveforms

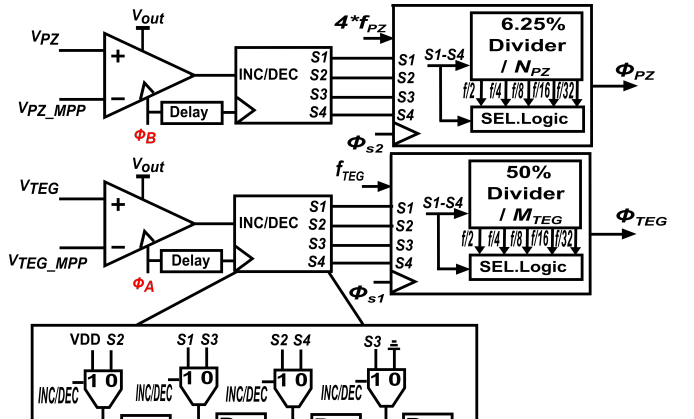
achieved by disabling the remaining low-frequency dividers through using a simple clock-gating technique.

B. Wide Range Zero Current Switching Circuit

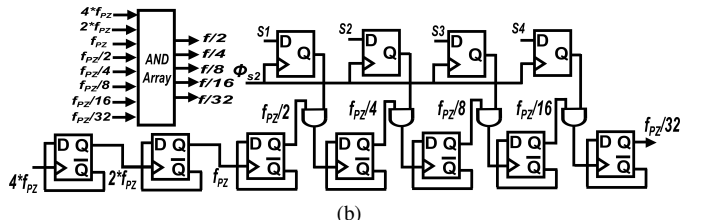
DC-DC converters working in DCM require an accurate control on inductor current while discharging in order to minimize inductor losses due to early or late switching [10], [11]. For seeking higher conversion efficiency, controlling ϕ_{off} for both sources with full-range varying input impedance at different load requirements is necessary [3], [6].

This paper presents a new technique for adjusting ϕ_{off} for both sources. From SPICE simulations, it is found that T_{off1} varies from 95 ns to 1.8 μ s for a TEG varying from 40 mV to 160 mV, also T_{off2} varies from 25 ns to 280 ns for a PZ varying from 0.8 V to 1.7 V. This range also covers more than a decade-variation in the load values.

As shown in Fig. 6, V_{ind} spikes are monitored and compared with V_{out} just after disengaging M_{p1} during both TEG and PZ harvesting cycles, then the output is latched and used to either increment or decrement $T0 - T15$ for TEG and $P0 - P15$ for PZ. A mux array with ϕ_{s2} as a selection bit is used to control either T_{off1} or T_{off2} . A digitally-tuned delay cell consists of 2-parallel inverters; one is strong with control signals V_{CTR} and \bar{V}_{CTR} and the other is weak, provides a delay of 25 ns to 30 ns delay during PZ cycle and from 95 ns to 105 ns delay during TEG cycle across all corners. A delay array employing



(a)



(b)

Fig. 5: (a) On-time control circuit for both TEG and PZ (b) 6.25% duty-cycle prog. dividers for PZ

this configurable delay cell is implemented and controlled by a thermometer code of 16-bit $Q0 - Q15$. The proposed circuit generates an output signal with pulse width varying from 180 ns to 2.8 μ s for TEG and from 19 ns to 700 ns for PZ.

In order to validate the proposed technique, V_{ind} and V_{out} are plotted in Fig. 7a for a TEG cell of 40 mV with $R_{TEG} = 2 \Omega$ and a PZ cell of 1.6 V with $R_{PZ} = 2 \text{ k}\Omega$. At steady-state, ϕ_{off} for both sources is toggled between 2 sub-optimal states every ϕ_{on} cycle as shown in Fig. 7b.

C. Output Regulation

In order to adjust output voltage, a regulation unit is adopted to provide a low-ripple dc output voltage which can be used to self bias the system once it reaches a steady state [12].

Coarse regulation scheme is implemented by always monitoring and comparing output voltage with a dedicated-voltage reference. The result is used in synchronous fashion with ϕ_{s1} to either enable or disable the wireless circuit as shown in Fig. 8. This technique will not affect sources operating voltages V_{TEG} and V_{PZ} , so maximum power extraction is always guaranteed while maintaining a quite regulated output.

In order to minimize system quiescent-power consumption, always-on blocks are designed to operate in sub-threshold increasing the ability of self-biased operation. Divided version of output voltage is generated with 1/5-voltage divider using a stack of PMOS transistors operating in sub-threshold consuming around 400 pA to drive relatively large input capacitance of always-on comparators.

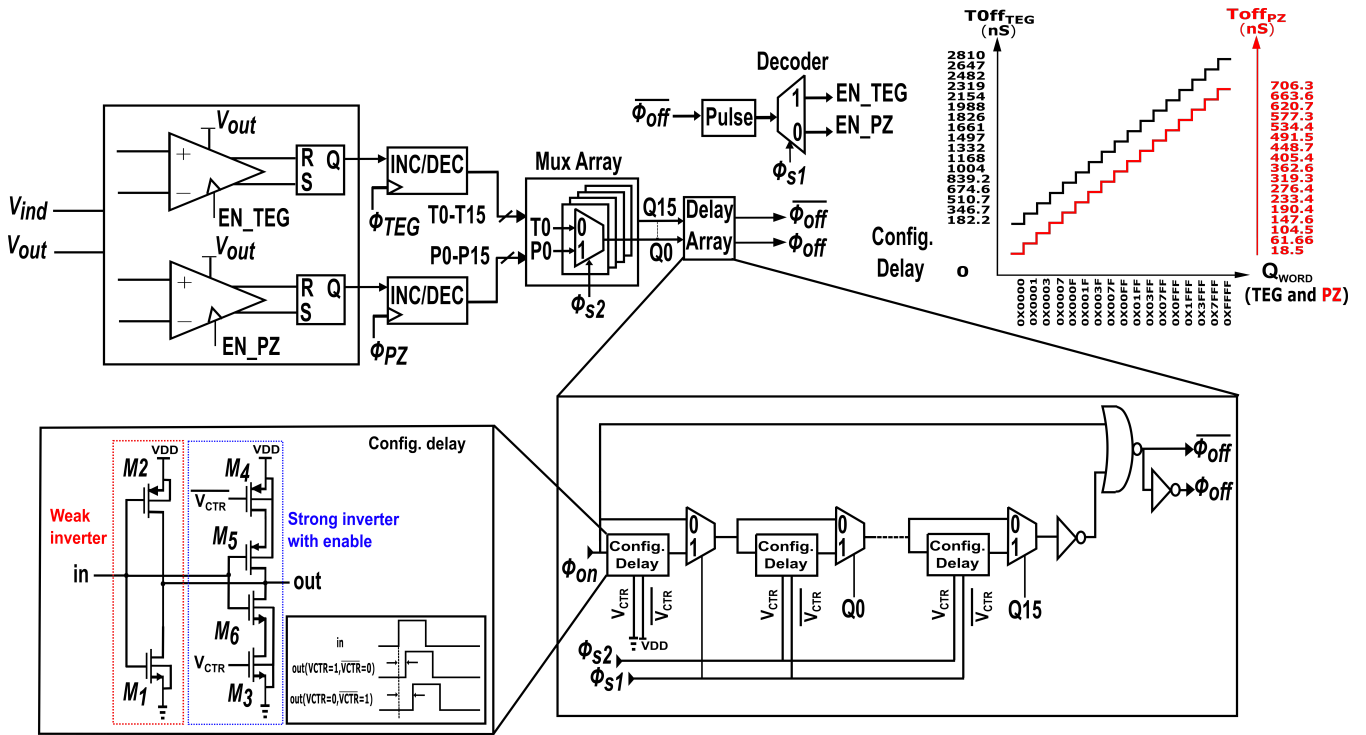


Fig. 6: Wide-Range Zero Current Detection circuit

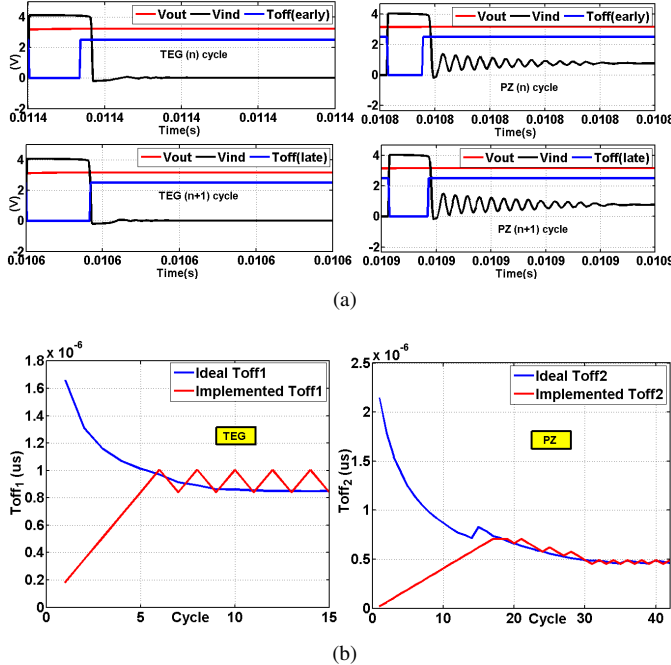


Fig. 7: (a) V_{ind} and V_{out} waveforms (b) ϕ_{off} signal for both sources at steady-state

A Band gap reference (BGR) circuit is designed to provide 0.5 V while consuming 8.3 nA. A continuous-time comparator is implemented using a 2-stage amplifier with a dedicated supply-independent current source of 20 nA.

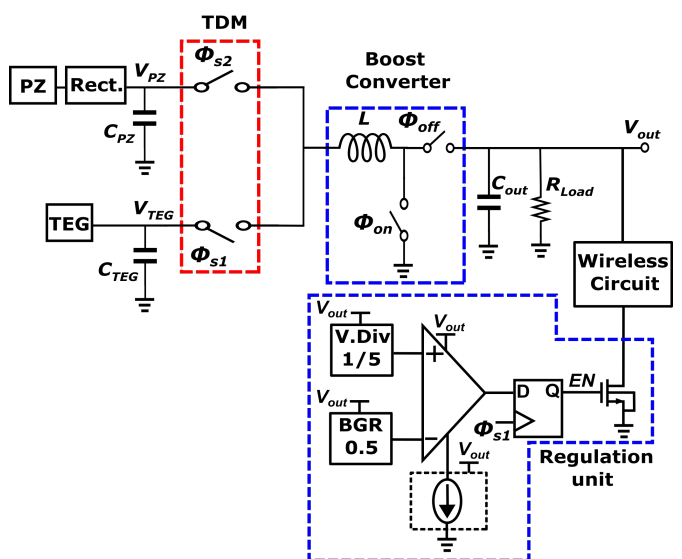


Fig. 8: Output regulation unit implementation

IV. SIMULATION RESULTS

A. Output results:

With the minimum energy available from the harvesters and with using an output capacitor of 2 μ F with an initial kick-start voltage of 2.3 V, system can reach steady-state operation generating a regulated output voltage of 2.5 V while driving a max power of 3.125 μ W.

In Fig. 9, BGR line regulation and the wireless-circuit enable signal are all illustrated. Moreover in the same figure, with $V_{TEG,OC} = 50$ mV and $V_{PZ,OC} = 0.8$ V and with R_{TEG} of $32\ \Omega$ and R_{PZ} of $32.768k\Omega$, system sustains a self-biased operation while V_{out} is charged and regulated at 2.5 V.

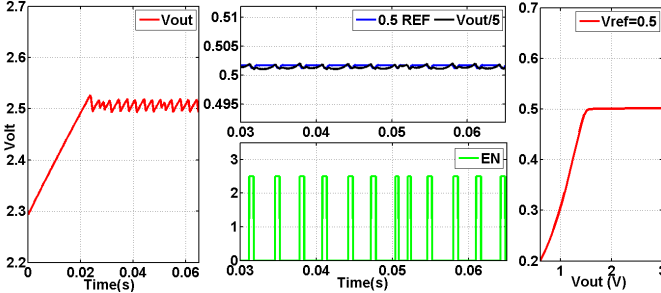


Fig. 9: Vout Regulation, BGR output and transmission enable signal

B. MPPT transient response:

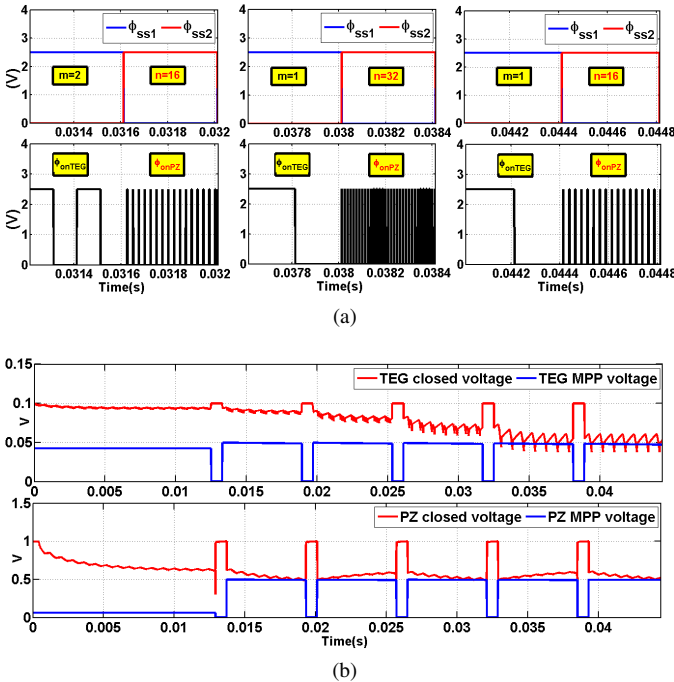


Fig. 10: (a) Searching For optimal m and n (b) Closed voltage of both harvesters with respect to generated MPP values

MPPT loop dynamics can be examined by using $V_{TEG,OC}$ and $V_{PZ,OC}$ of 100 mV and 1 V respectively with R_{TEG} of $2\ \Omega$ and R_{PZ} of $2048\ \Omega$. System always starts with max m and n in order to minimize the locking time when the harvesters are operating with their highest resistances. In Fig. 10a using f_{PZ} of 160 kHz and f_{TEG} of 80 kHz, system is locked at $m = 1$ while it fluctuates between $n = 16$ and $n = 32$.

TABLE II: Performance comparison summary

	This Work	[5]	[3]
Technology	$0.13\ \mu\text{m}$	$0.5\ \mu\text{m}$	$0.35\ \mu\text{m}$
Technique	inductive boost	inductive boost	inductive buck-boost
MPPT	Yes Dual-source	Yes TEG-array	Yes Hard-coded
MPPT Range	TEG 2 Ω - 32Ω PZ 2 $k\Omega$ - $44k\Omega$	TEG 33-2.7 $k\Omega$	TEG 4.1 Ω - 13Ω PV 30 Ω - 6.6 $k\Omega$ Piezo 11 $k\Omega$ - 350 $k\Omega$
Input Voltage	TEG 50 mV PZ 0.8 V	TEG 20 mV-160 mV PV 20mV-150mV	TEG 20 mV-160 mV PV 150 mV-750 mV Piezo 1.5 V - 5 V
Output Voltage	2.5 V	1.8-2.5 V	VLoad 1.8 V VStore 1.8 V-2.5 V
Quiescent Power	1 μW	1 μW	NA
ZCS	TEG (90 ns- $2.8\mu\text{s}$) PZ (15 ns- 750ns)	NA	NA

While searching for optimal m and n , closed voltages of both harvesters are dynamically changed till they reach their periodically sampled MPP values as shown in Fig. 10b.

Finally, Table II shows a comparison between this work and previous contributions.

V. CONCLUSION

This paper presents a new technique for tracking wide-range impedance variations for a dual-source energy harvesting system employing TDM technique between TEG and PZ harvesters. This technique achieves a global maximum power extraction using a dual-source MPPT unit. A novel digitally-based wide range delay chain is proposed and implemented in a boost DC-DC converter working in DCM to ensure proper off-switching instants for inductor current under different load requirements. Moreover, a coarse-regulation unit is adopted to control the steady-state output voltage while maintaining MPP operation. This work presents a mathematical model for the converter impedance at steady-state and verify this model against the simulation results at different harvesting conditions.

REFERENCES

- [1] S. Bandyopadhyay, P. P. Mercier, A. C. Lysaght, K. M. Stankovic, and A. P. Chandrakasan, "A 1.1nw energy harvesting system with 544pw quiescent power for next-generation implants," in *2014 IEEE International Solid-State Circuits Conference Digest of Technical Papers (ISSCC) 23.2*, Feb 2014, pp. 396-397.
- [2] Y. K. Ramadas and A. P. Chandrakasan, "A battery-less thermoelectric energy harvesting interface circuit with 35 mv startup voltage," *IEEE Journal of Solid-State Circuits*, vol. 46, no. 1, pp. 333-341, Jan 2011.

- [3] S. Bandyopadhyay and A. P. Chandrakasan, "Platform architecture for solar, thermal, and vibration energy combining with mppt and single inductor," *IEEE Journal of Solid-State Circuits*, vol. 47, no. 9, pp. 2199–2215, Sept 2012.
- [4] M. R. Elhebeary, M. A. A. Ibrahim, M. M. Aboudina, and A. N. Mohieldin, "A dual source microscale energy harvesting system for wireless sensor networks," in *2015 IEEE 24th International Symposium on Industrial Electronics (ISIE)*, June 2015, pp. 140–145.
- [5] S. Carreon-Bautista, A. Eladawy, A. N. Mohieldin, and E. Sanchez-Sinencio, "Boost converter with dynamic input impedance matching for energy harvesting with multi-array thermoelectric generators," *IEEE Transactions on Industrial Electronics*, vol. 61, no. 10, pp. 5345–5353, Oct 2014.
- [6] D. El-Damak and A. P. Chandrakasan, "A 10 nw- 1 uw power management ic with integrated battery management and self-startup for energy harvesting applications," *IEEE Journal of Solid-State Circuits*, vol. 51, no. 4, pp. 943–954, April 2016.
- [7] S. Stanzione, C. van Liempd, M. Nabeto, F. R. Yazicioglu, and C. V. Hoof, "A 500nw batteryless integrated electrostatic energy harvester interface based on a dc-dc converter with 60v maximum input voltage and operating from 1 uw available power, including mppt and cold start," in *2015 IEEE International Solid-State Circuits Conference - (ISSCC) Digest of Technical Papers* 20.8, Feb 2015, pp. 1–3.
- [8] O. Lopez-Lapena, M. T. Penella, and M. Gasulla, "A new mppt method for low-power solar energy harvesting," *IEEE Transactions on Industrial Electronics*, vol. 57, no. 9, pp. 3129–3138, Sept 2010.
- [9] A. Roy, A. Klinefelter, F. B. Yahya, and X. Chen, "A 6.45 murmW self-powered soc with integrated energy-harvesting power management and ulp asymmetric radios for portable biomedical systems," *IEEE Transactions on Biomedical Circuits and Systems*, vol. 9, no. 6, pp. 862–874, Dec 2015.
- [10] H. J. Chen, Y. H. Wang, P. C. Huang, and T. H. Kuo, "An energy-recycling three-switch single-inductor dual-input buck/boost dc-dc converter with 93peak conversion efficiency and 0.5mm² active area for light energy harvesting," in *2015 IEEE International Solid-State Circuits Conference - (ISSCC) Digest of Technical Papers* 20.9, Feb 2015, pp. 1–3.
- [11] P. H. Chen, C. S. Wu, and K. C. Lin, "A 50nw-to-10mw output power tri-mode digital buck converter with self-tracking zero current detection for photovoltaic energy harvesting," in *2015 IEEE International Solid-State Circuits Conference - (ISSCC) Digest of Technical Papers* 20.10, Feb 2015, pp. 1–3.
- [12] K. Kadirvel, Y. Ramadass, U. Lyles, J. Carpenter, and V. Ivanov, "A 330na energy-harvesting charger with battery management for solar and thermoelectric energy harvesting," in *2012 IEEE International Solid-State Circuits Conference*, Feb 2012, pp. 106–108.